Emergent atomistic Kondo resonances in strained carbon-benzene single chains

L. Craco and S. S. Carara
Institute of Physics, Federal University of Mato Grosso, 78060-900 Cuiabá, MT, Brazil

(Received 30 January 2020; revised manuscript received 3 April 2020; accepted 21 April 2020; published 6 May 2020)

Using real-space generalized gradient approximation plus dynamical mean-field theory (GGA + DMFT) we explore the effect of uniaxial strain on the correlated electronic structure reconstruction of atomistic carbon patterned out in carbon-benzene single chains. Firstly, based on GGA we show how strain can trigger a valley electronic structure with similarities akin to narrow-band semiconductors. The correlated electronic structure we derive is promising in the sense that it enables the observation of emergent Kondo quasiparticle resonances for future valleytronics based on low-dimensional organic conductors. Our proposal is a key step to iteratively understand the intricate and interdependent changes in orbital and electronic degrees of freedom at the atomistic level.

DOI: 10.1103/PhysRevB.101.205406

I. INTRODUCTION

The application of pressure and negative pressure (strain) are useful tools to tune structural and electronic properties of real materials [1]. The potential to tune structural, electronic, and magnetic properties of strained graphene, for example, has been explored in recent years both experimentally [2] and theoretically [3–5]. However, in spite of many efforts in understanding graphenelike systems, studies on strain-induced electronic structure reconstruction and the precise nature of the emergent coherent Kondo state [6] in carbon-based quasi-one-dimensional (quasi-1D) single chains [7] is still missing. With this caveat in mind, here we carried out real-space generalized gradient approximation plus dynamical mean-field theory (GGA + DMFT) [8] calculations to unveil atomistic electronic properties of normal and strained carbon-benzene (CB) single chains (see Fig. 1). The reconstructed electronic structure we derive captures Kondo features to be seen in future scanning tunneling microscopy (STM) experiments [6]. As a by-product we predict an emergent Kondo phenomenon in atomistic carbon (atomistic C) with characteristics akin to correlated multiorbital (MO) systems treated within DMFT [9].

It should be noted that reducing bulk graphite to two-dimensional graphene [10] has opened the possibility to explore novel low-dimensional (low-D) phenomena on organic conductors [11]. Interesting in this context are graphene nanoribbons [12] and carbon nanotubes [6,13]. Also relevant is the formation of atomic carbon chains from graphene nanoribbons [14], as well as the synthesis of linear chains of atomistic-conjugated benzene molecules [7,15]. Moreover, there had been a number of studies about the synthesis and stability of pure atomic carbon [16] and π-conjugate molecular chains [15,17,18], some of them which have already been experimentally observed [7,12,19]. However, in spite of many experimental and theoretical efforts, the important role played of uniaxial strain in quasi-1D organic systems remains unclear. Motivated thereby, in this work we reveal the interplay between strain-induced orbital differentiation [3] and MO electron-electron interactions in the electronic structure of the carbon analog of leucoemeraldine [15], showing emergent Kondo quasiparticle resonances [20] and electron mass enhancement within the atomistic clean limit.

The possibility of correlated electron physics in carbon-based materials [6,21–24] remains intriguing, since the naive expectation dictates that the itinerance (kinetic energy of p carriers) is appreciable compared to the electron-electron interactions, as distinct from d-band systems, where the d electrons reside in much narrower bands. Hence, the effective ratio between the on-site Coulomb repulsion and the one-particle bandwidth (U/W) is sizable. This controversy makes the possible relevance of intrinsic electron-electron interactions in organic metals and semimetals [25,26] or in polymeric materials [7,27] as well as to fullerenes, where $U/W \sim 1.5-2.5$ [21], an issue of living interest [28]. With this in mind, in this work we show how the interplay between broadband electronic delocalization and sizable on-site Coulomb repulsion [23] can induce a local electronic reconstruction with emergent Kondo quasiparticles [20,29] in strained, single-chain organic conductors. However, before delving into the correlated electronic state in atomistic C of normal and strained CB single chains, it is important to note that the bare (U_b) and screened (U_s) on-site, Coulomb interaction parameters for two-dimensional graphene (three-dimensional graphite) are, respectively, $U_b = 17.0$ eV and $U_s = 9.3$ eV ($U_b = 17.5$ eV and $U_s = 8.3$ eV) [23]. Owing to the insulating nature of elemental C, one would expect the local Coulomb interaction to be rather close to unscreened U_b values of graphene and graphite. With this in mind we numerically interpolate the Coulomb interaction parameters above as a function of dimensionality (D) to extract a realistic upper limit for the Coulomb interaction in each atomistic C linked to two nearest-neighbor benzene (B) rings. Within our fitting procedure (see Fig. 2) we predict a $U_s = 12.2$ eV for atomistic C in the quasi-1D limit of CB single chains. Therefore, in our study below we chose $U(\equiv U_s)$ values

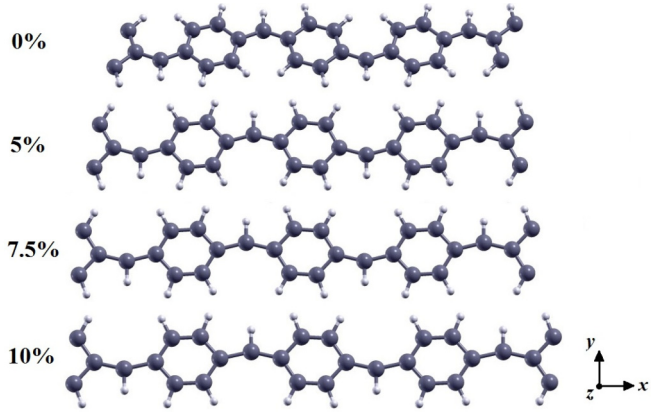

FIG. 1. Planar view showing the relaxed structure of normal and strained carbon-benzene (CB) single chains. Carbon and hydrogen atoms in these single chains are shown in dark and light colors, respectively. Notice the changes in the bonding angle with increasing uniaxial strain.

up to 12.0 eV to reveal the emergence of atomistic Kondo quasiparticle resonances in strained CB single chains at low energies.

II. RESULTS AND DISCUSSION

In order to gain realistic insights into the electronic and mechanical properties in quasi-1D CB single chains, in Fig. 3 we display orbital-resolved GGA results for the bare electronic structure of atomistic C patterned between two B molecules (see Fig. 1), showing how it can be partially reshaped by moderate uniaxial strain. Optimum geometry, stability, and one-particle electronic properties of the system were investigated within density-functional theory (DFT), as implemented in the SIESTA simulation package [30]. The unit cell of the CB single chain is composed of 24 atoms, where 14 of them are carbon atoms and the remaining being hydrogen atoms.

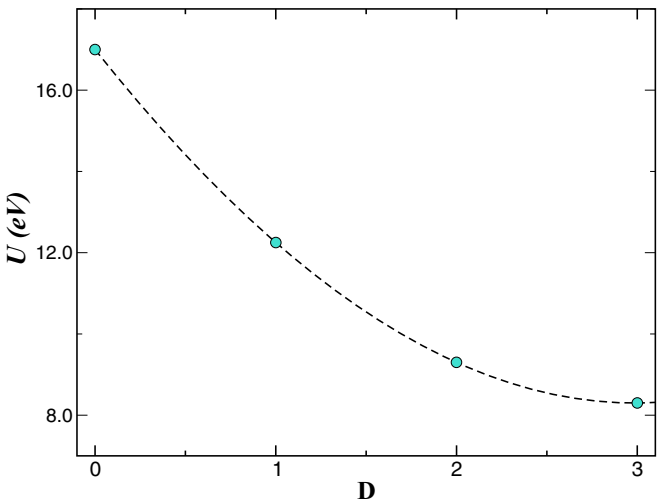

FIG. 2. On-site Coulomb interaction parameters as a function of dimensionality for carbon-based systems. U values for D = 0, 2, and 3 were taken from Ref. [23].

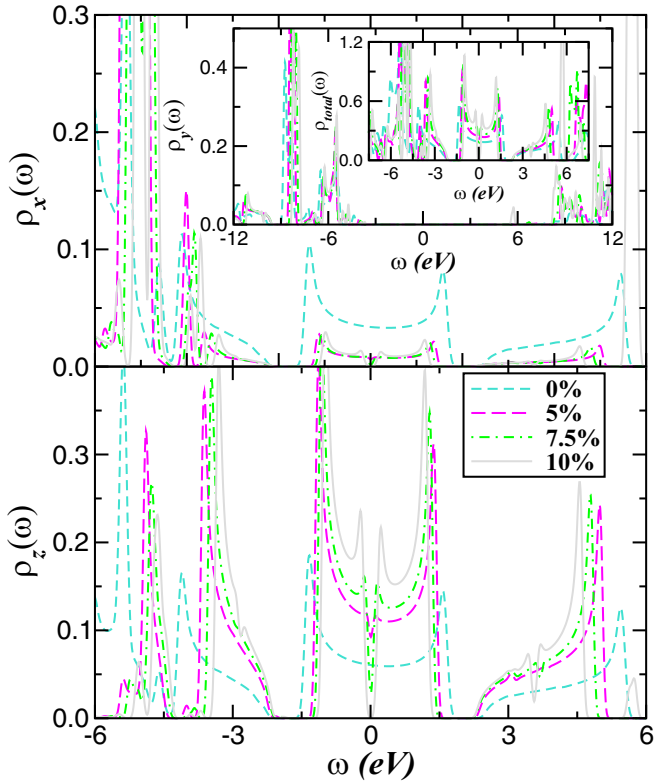

FIG. 3. GGA orbital-resolved and total density-of-states (DOS) of atomistic carbon (atomistic C) patterned between two benzene rings. Notice the large bonding-antibonding gap within the p_y orbital and the sharp singular peaks on all orbitals. Particular features to note is the narrow one-dimensional-like minibands with x, z orbital character near the Fermi level, $E_F = \omega = 0$, and the $x - z$ orbital differentiation with appearance of a bare one-particle band gap with increasing uniaxial strain.

The lattice parameter of the unstrained relaxed structure found in our GGA calculations is equal to 11.51 Å. The obtained C-C distance is 1.43 Å and the bonding angle between the two B molecules is equal to 134.4° for the normal relaxed (not stretched) structure. As shown in Fig. 1 the CB single chain is infinite along the x direction. To ensure that there is no interaction between successive periodic images we use a cell with vacuum space of 30 Å in the y, z directions. Moreover, to investigate the effect of uniaxial strain along the x direction the lattice parameter has been increased by 5%, 7.5%, and 10% of its unstrained value and the atomic positions were relaxed for each strained structure. The respective Brillouin zone is sampled by a $15 \times 5 \times 5$ Monkhorst-Pack grid [31]. The geometries were fully optimized until all the force components became smaller than 0.04 eV/Å. Norm-conserving pseudopotentials of Troullier-Martins [32] in Kleinman-Bylander nonlocal form were used to represent the ionic core potential. We use the GGA, as parametrized by Perdew *et al.* scheme [33], for the exchange-correlation functional. The Kohn-Sham orbitals [34] are expanded in a linear combination of atomic orbitals of finite range which is determined by a common confinement energy shift of 0.01 Ry [35]. The precision of the real-space grid integration is determined by a minimal energy cutoff of 200 Ry [36].

It can be observed in Fig. 3 that the bare GGA density of states (DOS) exhibits nondegenerate $2p_{x,z}$ bands crossing the Fermi energy ($E_F = \omega = 0$), implying the absence of true orbital Kondo effect [6,37] in this two-channel electron gas at normal and strained conditions. Within this quasi-1D structural configuration, the $p_{x,z}$ orbitals are equally found at each atomistic C along the single chain, displaying equivalent orbital-resolved DOS as in Fig. 3. While due to loss of translation symmetry the p_y orbital is insulating, the p_x orbital is slightly more localized as compared to the p_z channel near E_F in the unstrained regime. However, remarkable effects on the bare electronic structure are predicted to exist when the single-CB chain is stretched out of its relaxed atomic structure. Firstly, while the total DOS (see inset of Fig. 3) continuously enhances at energies up to ± 1.5 eV about E_F, strongly depleted electronic states are found in this narrow energy window within the p_x orbital sector upon stretching the single-CB chain (see upper main panel). Moreover, as shown in Fig. 3 (lower panel), an interestingly reverse trend sets in within the p_z channel. The overall p_x electronic depletion provides the electronic seeds to p_z DOS enhancement due to reduced xz rehybridization with increasing strain. Finally, also noteworthy are the van Hove singularities akin to 1D [29] and single-chain [38] systems close to ± 1.5 eV as well as the opening of a pseudoband gap at 5% strain, which continuously evolves towards a true one-particle band gap upon 10% stretching of the CB single chain as in Fig. 1. How this surprisingly low-in-energy electronic reconstruction with emergent quasi-1D minibands and narrow semiconducting band gaps relevant for future valleytronics [39] are reshaped by MO electron-electron interactions at the atomistic level is our focus here.

Consistent with an earlier study on C quantum dot patterned in graphene nanoflakes [8], the many-body Hamiltonian relevant at each atomistic C is $H = H_0 + H_{int}$, with $H_0 = \sum_{\mathbf{k}a\sigma} \varepsilon_a(\mathbf{k}) c^{\dagger}_{\mathbf{k}a\sigma} c_{\mathbf{k}a\sigma}$ and $H_{int} = U \sum_{ia} n_{ia\uparrow} n_{ia\downarrow} + \sum_{ia\neq b} U' n_{ia} n_{ib} - J_H \sum_{ia\neq b} \mathbf{S}_{ia} \cdot \mathbf{S}_{ib}$. Here, $a = x, y, z$ label the diagonalized p bands, and $\varepsilon_a(\mathbf{k})$ is the one-electron band dispersion projected on each atomistic C, which encodes details of its actual one-electron (GGA) band structure as well as its hybridization with the two neighboring B molecules. $U' \equiv U - 2J_H$, with U, U' being the intra- and interorbital Coulomb repulsion and J_H is the Hund's rule coupling [24]. The peculiar one-particle band structure of our relaxed atomistic C at normal and strained conditions are read off from the projected DOS shown in Fig. 3, which are GGA inputs for the MO-DMFT approach that reveals the coexistence of collective Kondo resonances [20] at low energies with high-in-energy Hubbard bands at 10% uniaxial strain.

To make progress towards understanding correlation-induced electronic reconstruction in atomistic C we use real-space DMFT [40], where each lattice site of a particular system is mapped onto its own impurity model. As in the usual DMFT treatment [29] this mapping is done by computing the local Green's function at each site $G^{loc}_a(\omega) = \frac{1}{N} \sum_{\mathbf{k}} \frac{1}{\omega - \Sigma_a(\omega) - \varepsilon_a(\mathbf{k})}$, where $\Sigma_a(\omega)$ is the corresponding momentum-independent self-energy, which encodes all many-particle correlation effects. To perform the $\mathbf{k}$ sum above, we shall make use of the Hilbert transform [29] and rewrite $G^{loc}_a(\omega)$ at each orbital a as

$$G^{loc}_a(\omega) = \int d\epsilon \frac{\rho^{GGA}_a(\epsilon)}{\omega - \Sigma_a\left(\left[\mathcal{G}^0_a(\omega)\right]\right) - \epsilon}. \quad (1)$$

Here, $\rho^{GGA}_a(\epsilon)$ are the bare DOS of atomistic C displayed in Fig. 3 and $\mathcal{G}^0_a(\omega)$ are the site-excluded Green's functions, usually referred to as Weiss functions [29]. Based on the fact that we use diagonalized one-particle spectral functions for DMFT, computation of Eq. (1) can be performed for all orbital-resolved Green's functions as well the corresponding bath propagators

$$\left[\mathcal{G}^0_a(\omega)\right]^{-1} = \left[G^{loc}_a(\omega)\right]^{-1} + \Sigma_a(\omega). \quad (2)$$

These site-excluded Green's functions are used to compute self-consistently $\Sigma_a(\omega)$ [41,42]. As already discussed in Ref. [8], Eqs. (1) and (2) form a closed set of coupled, nonlinear relations which are solved numerically until convergence is achieved. Importantly, the equations above are reduced to the usual DFT+DMFT treatment if atomistic C is replaced by a single site in the lattice problem [43].

Let us now discuss our GGA + DMFT results. To pinpoint the relevance of MO electron-electron interactions for the electronic reconstruction of normal and strained CB single chains at atomistic level, we compare in Fig. 4 the total GGA DOS with the GGA + DMFT results for two U values and fixed $J_H = 0.5$ eV (this choice for J_H is in accordance with values estimated for a local moment problem in graphene) [44] as well as fixed total electron occupancy $n = 3.0$. To trace the effect of dynamical MO interactions, e.g., the appearance of electronic structure reconstruction akin to MO Hubbard models treated within DMFT [9], in the upper panels of Fig. 4 we display the evolution of the total DOS for unstrained and 5%-strained CB single chains. One immediately notices in the upper panels of Fig. 4 that MO electron-electron interactions modify the bare GGA spectral functions of both at normal [45] and strained conditions: the latter being stronger due to enhanced U/W ratio triggered by strain-induced one-particle band narrowing. As common to correlated electron systems [9], MO dynamical correlations arising from U and U' lead to spectral weight redistribution from low to high energies, smearing out the sharp Van Hove singularities at the border of the minibands close to ± 1.5 eV. Moreover, while the semiconducting p_y orbital is not affected by MO electronic interactions (not shown), remarkable fingerprints of dynamical spectral weight transfer (SWT) are visible within the $p_{x,z}$ orbitals at energies close to ± 1.8 eV where the bare band gap is filled up with increasing U both at normal [45] and strained conditions. Particularly interesting is the salient narrowing of the emergent Kondo resonance [9,20,29] at low energies for $U = 12.0$ eV upon increasing strain. As visible, above 7.5% strain (see lower panel inset) the overall spectral line shape clearly deviates from that found in GGA near E_F. Remarkable as well is the band gap shrinkage at $U = 12.0$ eV for 10.0% strain and the appearance of a V-shaped metallic electronic state near E_F as well as the peak-deep-hump line shape [46] with clear shoulders in the quasiparticle peaks [9] at energies near to 1.1 eV above and below E_F, both arising from dynamical SWT. Thus, based on our results in Fig. 4, Kondo quasiparticle peaks are predicted to be seen

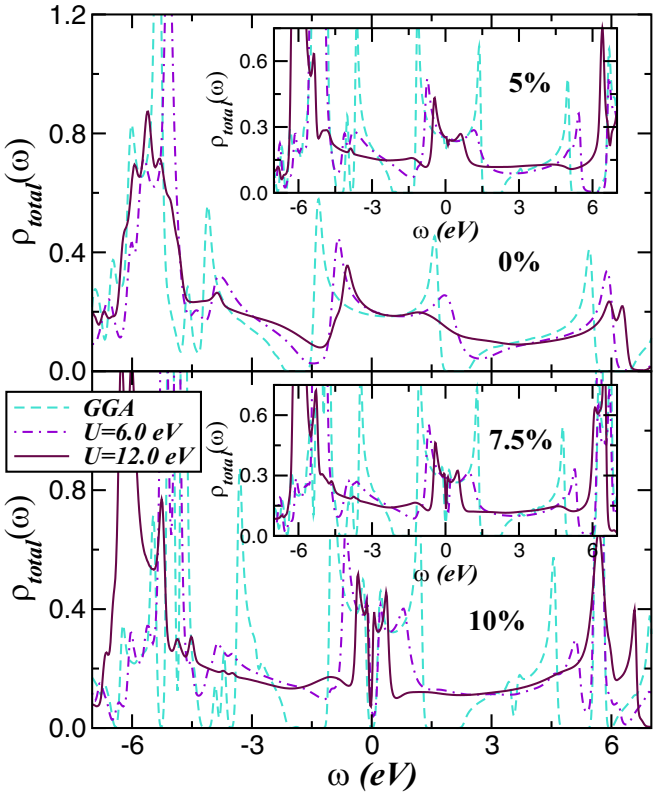

FIG. 4. Comparison between total GGA and GGA + DMFT results for electronic structure reconstruction of atomistic C, showing the interplay between uniaxial strain and on-site Coulomb repulsion effects. Notice the evolution of the total DOS with increasing strain and the emergence of narrow Kondo quasiparticles at low energies. Compared to the GGA results, large spectral weight transfer is visible in the reshaped GGA + DMFT spectral functions upon increasing U.

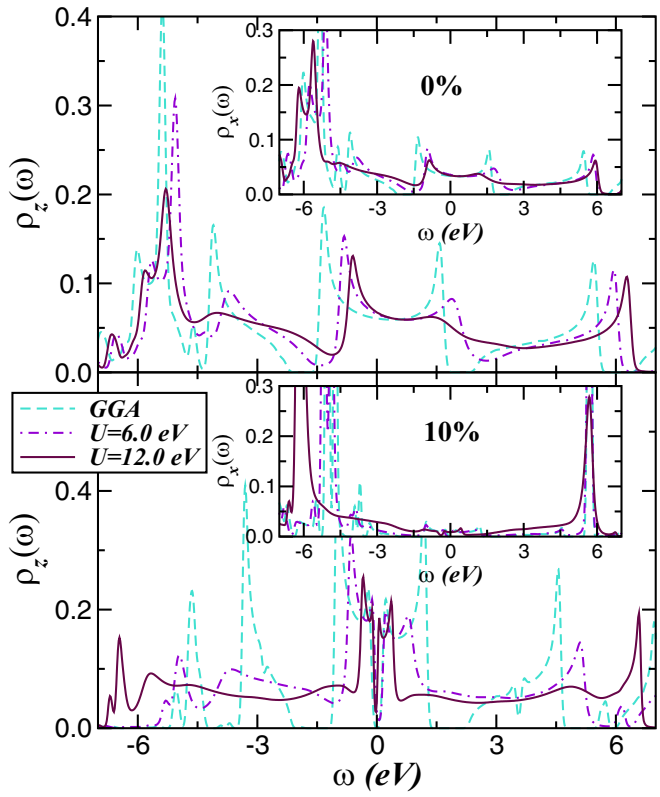

FIG. 5. Comparison between GGA and GGA + DMFT orbital-resolved spectral functions for the atomistic C. Notice the orbital differentiation induced by uniaxial strain and the emergence of the Kondo quasiparticle resonances at low energies with increasing the Coulomb interaction U. Noteworthy is the peak-deep-hump line shape with clear shoulders in the p_z quasiparticle peak at 10% strain.

in atomistic C with increasing strain at low temperatures, and future STM studies [6] are called for to corroborate this prediction.

In Fig. 5 we display the precise nature of strain-induced orbital differentiation [3] in atomistic C. For the sake of clarity let us concentrate first on our GGA results. As seen in the upper panel of Fig. 5, albeit the p_z DOS is higher, the two-metallic p-band channels of atomistic C have appreciable weight near E_F within the unstrained regime. As already pointed out in our discussion of Fig. 4 above, we find an interesting orbital differentiation where the p_x spectral function near E_F vanishes while the p_z DOS is enhanced near E_F with increasing strain. This electronic reconstruction we derive is consistent with earlier first-principles calculations of 30% strained graphene, showing that when uniaxial strain increases along a particular direction, the Fermi velocity (v_F) parallel to it decreases quickly, whereas perpendicular to it v_F increases by as much as 25% [3]. Thus, it follows that only residual electronic states are found along the chain direction (see the lower inset of Fig. 5), implying almost vanishing dynamical electron-electron interactions in the p_x orbital sector at 10% strain. The reverse trend is observed for the p_z orbital, where intraorbital electron interactions are promoted due to enhanced bare miniband DOS near E_F. Hence, as visible in the lower main panel of Fig. 5, appreciable dynamical SWT from low to high energies sets in with increasing U. Noteworthy are the incoherent Hubbard bands near to ± 5 eV and the shoulders above the quasiparticle peak [9] at energies close to ± 1.1 eV in the correlated p_z spectral function for $U = 12.0$ eV. The origin of these resonance shoulders is linked to the inverted slope and the kink [9] in the real part of p_z self-energy (see Fig. 6). The latter is also seen in the self-energy imaginary part [$\mathrm{Im}\Sigma_z(\omega)$], since both are known to be related by Kramers-Kronig transform. Thus, given the reduced electron correlation effects in the p_x as compared to the p_z orbital, the nature of the narrow Kondo resonance at $U = 12.0$ eV is mainly due to intraorbital SU(2) spin-Kondo effect [9], which is slightly enhanced via residual U'-induced MO correlation effects [37] at low temperatures.

It is noteworthy that close to half-filling the spectrum the Hubbard model as well as the Anderson impurity model (with noninteracting conduction bands) can be separated into two distinct features: the high-energy features are given by the incoherent (upper and lower) Hubbard bands which are well separated from the narrow Kondo resonance at the Fermi level [29], whose spectral weight tends to zero with increasing the U/W ratio. As seen in Figs. 4 and 5 this dynamical

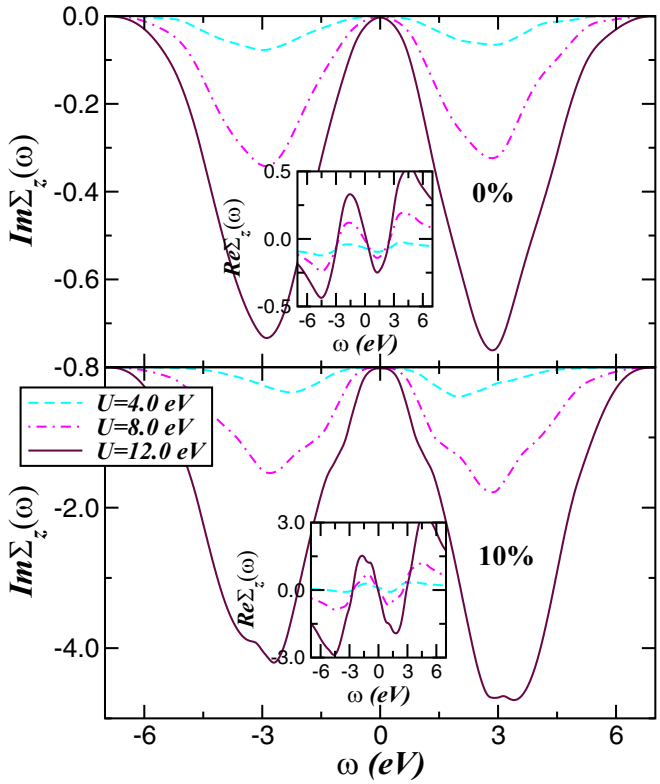

FIG. 6. Effect of electron-electron interaction within the p_z-orbital self-energy imaginary (main panels) and real (insets) parts, showing characteristics akin to good Landau Fermi-liquid metals [29] at low energies. Notice the inverted slope [9] near ± 1.1 eV in $\mathrm{Re}\Sigma_z(\omega)$ triggered by $U = 12.0$ eV at 10% strain.

transfer of spectral weight from low to high energies is well reproduced within the real-space GDA+DMFT scheme. However, to show the ability of real-space GGA + DMFT to capture Kondo-like physics, which builds up the Landau Fermi-liquid quasiparticles [29] at low energies, in Fig. 7 we display both the strain (main panel) and the U (inset) dependence of the half-width [47] (HW) of the quasiparticle resonances which can be interpreted as the low-energy coherence scale, usually referred to as Kondo temperature [29], below which the Landau Fermi-liquid description of the low-energy properties is obtained. Interestingly, both curves follow the same scaling behavior, implying a constant value for $\Delta \equiv \Gamma U$ [48] (with Γ being the coupling strength between atomistic C and the surrounding CB chains; leads in the context of Anderson impurity model) [48,49] and, thus, the emergence of a universal scaling function [48] upon increasing strain or on-site Coulomb correlations effects in atomistic C.

Finally, to more deeply understand the implications of strain-induced atomistic orbital differentiation, we recall that in DMFT the quasiparticle residue Z_a, which defines the renormalized Fermi energy of an orbital a, directly yields the effective mass of quasiparticles [29], $\frac{m_a^*}{m_e} = \frac{1}{Z_a} = (1 - \frac{\partial \mathrm{Re}\Sigma_a(\omega)}{\partial \omega})_{\omega=0}$, where m_e is the free-electron mass. Thus, from the slope of the self-energy real parts at E_F we obtain an orbital-dependent effective mass ratio $\frac{m_z^*}{m_e}$ for the three different U values used in Fig. 6. At 0% strain we obtain $\frac{m_z^\star}{m_e} = (1.02, 1.12, 1.29)$ for $U = (4.0, 8.0, 12.0)$ eV. These values increase monotonically with uniaxial strain, such that the overall electron mass enhancement at 10% strain is found to be $\frac{m_z^\star}{m_e} = (1.1, 1.61, 2.64)$. Interestingly, the effective band mass renormalization we derive is in qualitative good accord with experimental determined values $\frac{m^*}{m_e} \approx 1.25(\pm 0.03)$ for Na metal [50] as well to metallic black phosphorus, where $\frac{m^*}{m_e} = 1.38$ [51]. Additionally, for $U = 10.0$ eV and 10% strain we obtain $\frac{m_z^*}{m_e} = 2.04$, a value which is close to that found for $(\mathrm{BEDT\text{-}TTF})_3\mathrm{Br}(\mathrm{pBIB})$ (effective mass $\frac{m^*}{m_e} = 1.9$) [26], implying similar electron correlation effects in these low-D organic metals in spite of different material-specific properties and negative pressure conditions. Thus, taken together with earlier studies [26,50,51], our results in Figs. 5 and 6 certify the importance of treating dynamical, frequency-dependent correlation effects for understanding intrinsic low-energy electronic structure reconstruction and orbital differentiation of real broadband conducting systems [52].

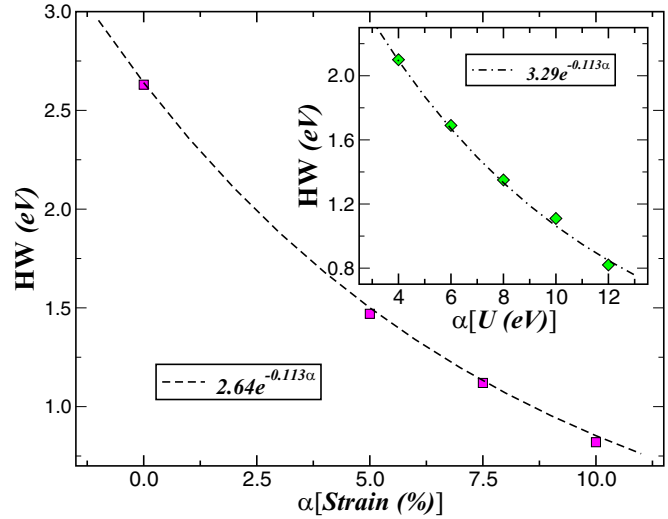

FIG. 7. Half-width (HW) of the p_z quasiparticle peak as a funtion of strain (main panel) and on-site Coulomb interaction (inset), showing a universal scaling behavior [48].

III. CONCLUSION

In summary, based on GGA and real-space GGA + DMFT calculations we have studied the electronic structure reconstruction and strain-induced orbital differentiation [3] of interacting local carbon atoms arranged on a quasi-1D carbon-benzene chain. We illustrate that even in a relatively simple geometry a variety of intricate many-particle effects, including the coherent state responsible for the emergence of Kondo quasiparticle resonances [9,20], is realized in broadband systems. Our study provides a useful guide for future experiments on quasi-1D polymeric single chains [7], and more generally, highlights the utility of real-space DFT+DMFT [8] as a fertile platform to explore novel physical phenomena in real materials at the atomistic level. A key advantage of real-space DFT+DMFT is its ability to iteratively

uncover many-body physics with highly tunable kinetic energy and local interaction strength from low to high energies at the atomistic level, revealing relevant physics at each energy scale.

ACKNOWLEDGMENTS

L.C.'s work is supported by CNPq (Grant No. 304035/2017-3). Acknowledgment (L.C. and S.S.C.) is also made to CAPES.

[1] M. Imada, A. Fujimori, and Y. Tokura, Rev. Mod. Phys. **70**, 1039 (1998).

[2] C. Lee, X. Wei, J. W. Kysar, and J. Hone, Science **321**, 385 (2008); N. Ferralis, R. Maboudian, and C. Carraro, Phys. Rev. Lett. **101**, 156801 (2008); M. L. Teague, A. P. Lai, J. Velasco, C. R. Hughes, A. D. Beyer, M. W. Bockrath, C. N. Lau, and N.-C. Yeh, Nano Lett. **9**, 2542 (2009); K. S. Kim, Y. Zhao, H. Jang, S. Y. Lee, J. M. Kim, K. S. Kim, J.-H. Ahn, P. Kim, J.-Y. Choi, and B. H. Hong, Nature (London) **457**, 706 (2009); N. Levy, S. A. Burke, K. L. Meaker, M. Panlasigui, A. Zettl, F. Guinea, A. H. Castro Neto, and M. F. Crommie, Science **329**, 544 (2010); N. N. Klimov, S. Jung, S. Zhu, T. Li, C. A. Wright, S. D. Solares, D. B. Newell, N. B. Zhitenev, and J. A. Stroscio, *ibid.* **336**, 1557 (2012).

[3] S.-M. Choi, S.-H. Jhi, and Y.-W. Son, Phys. Rev. B **81**, 081407(R) (2010).

[4] G. Gui, J. Li, and J. Zhong, Phys. Rev. B **78**, 075435 (2008); V. M. Pereira and A. H. Castro Neto, Phys. Rev. Lett. **103**, 046801 (2009); F. M. D. Pellegrino, G. G. N. Angilella, and R. Pucci, Phys. Rev. B **81**, 035411 (2010); **84**, 195404 (2011); J. H. Warner, E. R. Margine, M. Mukai, A. W. Robertson, F. Giustino, and A. I. Kirkland, Science **317**, 209 (2012); B. Amorim, A. Cortijo, F. de Juan, A. G. Grushin, F. Guinea, A. Gutiérrez-Rubio, H. Ochoa, V. Parente, R. Roldán, P. San-José, J. Schiefele, M. Sturla, and M. A. H. Vozmediano, Phys. Rep. **617**, 1 (2016); Z. Bi, N. F. Q. Yuan, and L. Fu, Phys. Rev. B **100**, 035448 (2019).

[5] L. Craco, D. Selli, G. Seifert, and S. Leoni, Phys. Rev. B **91**, 205120 (2015); L. Craco, S. S. Carara, and S. Leoni, *ibid.* **94**, 165168 (2016).

[6] P. Jarillo-Herrero, J. Kong, H. S. J. van der Zant, C. Dekker, L. P. Kouwenhoven, and S. de Franceschi, Nature (London) **434**, 484 (2005).

[7] A. J. Heeger, Rev. Mod. Phys. **73**, 681 (2000).

[8] L. Craco, S. S. Carara, T. A. da Silva Pereira, and M. V. Milošević, Phys. Rev. B **93**, 155417 (2016).

[9] F. B. Kugler, S.-S. B. Lee, A. Weichselbaum, G. Kotliar, and J. von Delft, Phys. Rev. B **100**, 115159 (2019).

[10] K. S. Novoselov, A. K. Geim, S. V. Morozov, D. Jiang, Y. Zhang, S. V. Dubonos, I. V. Grigorieva, and A. A. Firsov, Science **306**, 666 (2004).

[11] C. J. Brabec, N. S. Sariciftci, and J. C. Hummelen, Adv. Funct. Mater. **11**, 15 (2001).

[12] See, for example, O. V. Yazyev, Acc. Chem. Res. **46**, 2319 (2013); C. Cantillano, S. Mukherjee, L. Morales-Inostroza, B. Real, G. Cáceres-Aravena, C. Hermann-Avigliano, R. R. Thomson, and R. A. Vicencio, New J. Phys. **20**, 033028 (2018), and references therein.

[13] H. E. Troiani, M. Miki-Yoshida, G. A. Camacho-Bragado, M. A. L. Marques, A. Rubio, J. A. Ascencio, and M. Jose-Yacaman, Nano Lett. **3**, 751 (2003).

[14] E. Hobi, Jr., R. B. Pontes, A. Fazzio, and A. J. R. da Silva, Phys. Rev. B **81**, 201406(R) (2010).

[15] Zh. A. Boeva and V. G. Sergeyev, Polymer Science Series C **56**, 144 (2014).

[16] S. G. Kim, Y. H. Lee, P. Nordlander, and D. Tománek, Chemical Physics Letters **264**, 345 (1997).

[17] S. Hiroto, Chem. - Asian J. **14**, 2514 (2019).

[18] J. A. Januszewski and R. R. Tykwinski, Chem. Soc. Rev. **43**, 3184 (2014).

[19] C. Jin, H. Lan, L. Peng, K. Suenaga, and S. Iijima, Phys. Rev. Lett. **102**, 205501 (2009); A. Chuvilin, J. C. Meyer, G. Algara-Siller, and U. Kaiser, New J. Phys. **11**, 083019 (2009).

[20] G. D. Scott and D. Natelson, ACS Nano **4**, 3560 (2010).

[21] J. E. Han, E. Koch, and O. Gunnarsson, Phys. Rev. Lett. **84**, 1276 (2000); see also, P. Durand, G. R. Darling, Y. Dubitsky, A. Zaopo, and M. J. Rosseinsky, Nat. Mater. **2**, 605 (2003).

[22] R. L. Frank and E. H. Lieb, Phys. Rev. Lett. **107**, 066801 (2011).

[23] T. O. Wehling, E. Şaşıoğlu, C. Friedrich, A. I. Lichtenstein, M. I. Katsnelson, and S. Blügel, Phys. Rev. Lett. **106**, 236805 (2011).

[24] L. Craco, M. S. Laad, S. Leoni, and A. S. de Arruda, Phys. Rev. B **87**, 155109 (2013).

[25] V. N. Kotov, B. Uchoa, V. M. Pereira, F. Guinea, and A. H. Castro Neto, Rev. Mod. Phys. **84**, 1067 (2012).

[26] T. Kiss, A. Chainani, H. M. Yamamoto, T. Miyazaki, T. Akimoto, T. Shimojima, K. Ishizaka, S. Watanabe, C.-T. Chen, A. Fukaya, R. Kato, and S. Shin, Nat. Commun. **3**, 1089 (2012).

[27] H. T. Nicolai, M. Kuik, G. A. H. Wetzelaer, B. de Boer, C. Campbell, C. Risko, J. L. Brédas, and P. W. M. Blom, Nat. Mater. **11**, 882 (2012).

[28] M.-Q. Ren, S. Han, S.-Z. Wang, J.-Q. Fan, C.-L. Song, X.-C. Ma, and Q.-K. Xue, arXiv:1911.08768.

[29] A. Georges, G. Kotliar, W. Krauth, and M. J. Rozenberg, Rev. Mod. Phys. **68**, 13 (1996).

[30] J. M. Soler, E. Artacho, J. D. Gale, A. Garc'ıa, J. Junquera, P. Ordejón, and D. Sánchez-Portal, J. Phys.: Condens. Matter **14**, 2745 (2002); E. Artacho, E. Anglada, O. Diéguez, J. D. Gale, A. García, J. Junquera, M. Martin, P. Ordejón, J. M. Pruneda, D. Sánchez-Portal, and J. M. Soler, *ibid.* **20**, 064208 (2008).

[31] H. J. Monkhorst and J. D. Pack, Phys. Rev. B **13**, 5188 (1976).

[32] N. Troullier and J. L. Martins, Phys. Rev. B **43**, 1993 (1991).

[33] J. P. Perdew, K. Burke, and M. Ernzerhof, Phys. Rev. Lett. **77**, 3865 (1996).

[34] W. Kohn and L. J. Sham, Phys. Rev. **140**, A1133 (1965).

[35] J. Junquera, Ó. Paz, D. Sánchez-Portal, and E. Artacho, Phys. Rev. B **64**, 235111 (2001).

[36] J. Moreno and J. M. Soler, Phys. Rev. B **45**, 13891 (1992).

[37] L. Craco, M. S. Laad, and E. Müller-Hartmann, Phys. Rev. Lett. **90**, 237203 (2003).

[38] S. Meyer, T. Pham, S. Oh, P. Ercius, C. Kisielowski, M. L. Cohen, and A. Zettl, Phys. Rev. B **100**, 041403(R) (2019);

T. Pham, S. Oh, S. Stonemeyer, B. Shevitski, J. D. Cain, C. Song, P. Ercius, M. L. Cohen, and A. Zettl, arXiv:2001.06565.

[39] J. R. Schaibley, H. Yu, G. Clark, P. Rivera, J. S. Ross, K. L. Seyler, W. Yao, and X. Xu, Nat. Rev. Mater. **1**, 16055 (2016).

[40] R. Peters and N. Kawakami, Phys. Rev. B **92**, 075103 (2015).

[41] L. Craco, Phys. Rev. B **77**, 125122 (2008).

[42] To obtain the self-energy of each central carbon we use MO–iterated perturbation theory (MO-IPT) as an impurity solver. The detailed formulation of MO-IPT for correlated electron systems has already been developed [41] and used in the context of carbon-based materials [5, 24], so we do not repeat the equations used to compute $\Sigma_a(\omega)$ here.

[43] G. Kotliar, S. Y. Savrasov, K. Haule, V. S. Oudovenko, O. Parcollet, and C. A. Marianetti, Rev. Mod. Phys. **78**, 865 (2006).

[44] M. Casartelli, S. Casolo, G. F. Tantardini, and R. Martinazzo, Phys. Rev. B **88**, 195424 (2013).

[45] The detailed electronic structure reconstruction of unstrained CP single chains upon consideration of electronic interactions and particle-hole doping will appear elsewhere.

[46] A. A. Kordyuk, S. V. Borisenko, T. K. Kim, K. A. Nenkov, M. Knupfer, J. Fink, M. S. Golden, H. Berger, and R. Follath, Phys. Rev. Lett. **89**, 077003 (2002).

[47] Y.-H. Zhang, S. Kahle, T. Herden, C. Stroh, M. Mayor, U. Schlickum, M. Ternes, P. Wahl, and K. Kern, Nat. Commun. **4**, 2110 (2013).

[48] F. D. M. Haldane, Phys. Rev. Lett. **40**, 416 (1978).

[49] See also, L. Craco and K. Kang, Phys. Rev. B **59**, 12244 (1999).

[50] E. Jensen and E. W. Plummer, Phys. Rev. Lett. **55**, 1912 (1985); I.-W. Lyo and E. W. Plummer, *ibid.* **60**, 1558 (1988).

[51] N. Ehlen, A. Sanna, B. V. Senkovskiy, L. Petaccia, A. V. Fedorov, G. Profeta, and A. Grüneis, Phys. Rev. B **97**, 045143 (2018).

[52] L. Craco and S. Leoni, Phys. Rev. B **100**, 115156 (2019).